Proc. Natl. Acad. Sci. USA
Vol. 87, pp. 4849–4853, June 1990
Biochemistry

Crystal structure of an active form of RAS protein, a complex of a GTP analog and the HRAS p21 catalytic domain

(RAS protein/G protein/signal transduction/GTP complex of p21)

AXEL T. BRÜNGER*, MICHAEL V. MILBURN†, LIANG TONG†‡, ABRAHAM M. DEVOS†§, JARMILA JANCARIK†, ZIRO YAMAIZUMI¶, SUSUMU NISHIMURA¶, EIKO OHTSUKA‖, AND SUNG-HOU KIM†**

*Howard Hughes Medical Institute and Department of Molecular Biophysics and Biochemistry, Yale University, New Haven, CT 06511; †Department of Chemistry and Lawrence Berkeley Laboratory, University of California, Berkeley, CA 94720; ¶Biology Division, National Cancer Center Research Institute, Tokyo, Japan; and ‖Faculty of Pharmaceutical Sciences, Hokkaido University, Sapporo, Japan

Communicated by Melvin Calvin, March 2, 1990

ABSTRACT **Normal RAS proteins play a key role of molecular switch in the transduction of the growth signal from extracellular to intracellular space. The state of the switch is "on" when GTP is bound and "off" when GDP is bound to the protein. The crystal structure of a complex between a nonhydrolyzable GTP analog and the catalytic domain of a RAS protein has been determined by a rotation–translation search method. The orientations and positions of four independent molecules have been determined using a single molecule as a probe in the search. The crystal structure reveals that the γ phosphate of the GTP analog induces extensive conformational changes on two loop regions of the protein.**

RAS protooncogenes are essential for the cell's growth and survival and code for 21-kDa proteins, p21. There are three different *RAS* protooncogenes located in three different human chromosomes, and the protein sequences encoded by these genes are practically identical except for the C-terminal 25 residues (1). In analogy to elongation factor EF-Tu (2) and G proteins (3, 4), GTP-complexed RAS proteins are recognized by effector protein(s) as "on" state, signaling cell growth or differentiation, whereas the GDP complexes are perceived as the signal "off" state. RAS proteins have an intrinsic GTPase activity to turn off the signal, and this process is enhanced by GTPase activating protein, GAP (5–7).

We have previously determined the crystal structures of the GDP complex of a *RAS* protooncogene product and of a transforming mutant, both lacking the 18 C-terminal residues (8–10). To find out the mechanism of molecular switching, we have determined the crystal structure of a complex between a nonhydrolyzable GTP analog, guanosine-5′-(β,γ-methylene)-triphosphate (GDP[β,γ-CH_2]P), and the normal HRAS protein lacking the C-terminal 18 residues by using a new molecular replacement method. The structure is refined at 2.5-Å resolution with a current *R* factor of 19.5%. The structure reveals that an extensive conformational change is induced by the presence of the γ phosphate of GDP[β,γ-CH_2]P, which establishes additional hydrogen bonding interactions with two separate loop regions of the protein. At present resolution and state of refinement, except residues 62–65, the overall structural features are similar to the structure of the complex between RAS protein lacking the C-terminal 23 residues complexed with another nonhydrolyzable GTP analog, guanosine-5′-(β,γ-imido)triphosphate (GDP[β,γ-NH]P) and refined to 22.9% by using 10.0- to 2.6-Å resolution data (11).

Cloning, expression, and purification of the protein have been described earlier (12). The *Escherichia coli*-expressed protein contained GDP. To exchange this for the nonhydrolyzable GTP analog, GDP[β,γ-CH_2]P, the GDP complex at 2.4 mg/ml was incubated in a solution containing 20 mM EDTA, apyrase at 2.7 units/ml, and GDP[β,γ-CH_2]P at 0.17 mg/ml at 37°C for 15 min; then 1 M $MgSO_4$ solution was added to 33 mM. The mixture was concentrated, excess GDP[β,γ-CH_2]P was removed, and a buffer solution containing 50 mM Hepes, pH 7.5/1 mM EDTA/1 mM dithiothreitol/0.001% 1-octylglucoside was added. The last step was repeated twice, and the final solution was stored in 20% (vol/vol) glycerol.

For crystallization the GDP[β,γ-CH_2]P complex solution was dialyzed extensively against a solution containing 50 mM cacodylate buffer, pH 6.5/1 mM dithiothreitol/1 mM EDTA/0.01% 1-octylglucoside and concentrated to 14 mg of protein per ml in the same buffer. Crystals were obtained from a solution containing GDP[β,γ-CH_2]P complex at 7 mg/ml, 100 mM magnesium acetate, 10% (vol/vol) polyethylene glycol 8000, and 75 mM cacodylate buffer, pH 6.5, by vapor-phase equilibrium methods. The space group of the crystals is $P2_1$ (*c* unique) with unit cell parameters of $a = 41.5$ Å, $b = 80.1$ Å, $c = 130.5$ Å, and $\gamma = 117.5°$. Density measurement of GDP[β,γ-CH_2]P complex crystals suggested that there are three or four GDP[β,γ-CH_2]P complex molecules per asymmetric unit of the crystal. Most crystals were layered with each layer slightly misoriented with respect to its neighbors. X-ray diffraction data were collected on Kodak DEF5 films using a synchrotron x-ray source at the Brookhaven National Laboratory. The x-ray wavelength for the data collection was 1.22 Å, and the crystal-to-film distance was 90 mm. All data were collected at 4°C by using an Enraf-Nonius rotation camera. The films were scanned and digitized with an Optronix film scanner (Chelmsford, MA) at a resolution of 100 μm. The digitized data were processed by using computer programs originally written by Rossmann (13), and the reflections were reduced and merged by using the PROTEIN program package (14). The entire data set was collected on one crystal. During the data collection we searched for and irradiated the nonmultiple portion of a crystal. A total of 74,084 observations were made to a resolution of 2.5 Å, which reduced to give 21,061 unique reflections. Average $R_{sym}(I)$ was 6.1% and $R_{merge}(I)$ was 8.8%.

Structure Determination

Conventional rotation–translation search methods (15) did not provide a unique solution, although one (possibly two) of

The publication costs of this article were defrayed in part by page charge payment. This article must therefore be hereby marked "*advertisement*" in accordance with 18 U.S.C. §1734 solely to indicate this fact.

Abbreviations: PC, Patterson correlation; GAP, GTPase activating protein; GDP[β,γ-CH_2]P, guanosine-5′-(β,γ-methylene)triphosphate; GDP[β,γ-NH]P, guanosine-5′-(β,γ-imido)triphosphate.

‡Present address: Department of Biological Sciences, Purdue University, West Lafayette, IN 47907.
§Present address: Department of Biomolecular Chemistry, Genentech, Inc., South San Francisco, CA 94080.
**To whom reprint requests should be addressed.

the four rotation solutions was identified in retrospect. This is understandable because there are three or four molecules in an asymmetric unit. By applying a more recently developed molecular-replacement method (16) the structure was successfully solved.†† A brief description of the steps taken follows.

Rotation Search. (*i*) A self-rotation search was performed to locate noncrystallographic symmetry elements using a real-space Patterson search method (17). The Patterson map was calculated on a 1-Å grid by using all reflections from 15- to 4-Å resolution. Patterson vectors were selected according to length (between 24 and 5 Å). The selected Patterson vectors were rotated using the spherical polar angles (ψ, ϕ, κ), and the product correlation with the Patterson map was computed by linear eight-point interpolation. The self-rotation search was carried out by varying ψ and ϕ in steps of 2° in the angular range ψ = 0° to 180° and ϕ = 0° to 180°, while κ was held fixed at 180°. Apart from the crystallographic diad at ψ = 90°, a strong noncrystallographic 2-fold axis emerges at ψ = 60°, ϕ = 0°, and three other positions (ψ = 150°, ϕ = 0°; ψ = 30°, ϕ = 180°; ψ = 120°, ϕ = 180°) that are related to each other by crystallographic symmetry. This strong, unique peak suggests that there is an even number of molecules, four rather than three, in the asymmetric unit, and that the four molecules form two dimers where the monomers in each dimer (or the two dimers) are related by the noncrystallographic 2-fold axis. A search for a noncrystallographic 4-fold axis did not produce a unique symmetry element.

(*ii*) We performed a rotation search using the crystal structure of GDP complex of the catalytic domain of normal p21 protein (8, 10) as a probe structure. The GDP and residues 30–40 and 60–70 (near the expected γ-phosphate location) were deliberately removed from the probe. The rotation search using the partial structure of the GDP complex as probe was repeated with a real-space Patterson search method (17). The model Patterson maps were computed by placing the probe model into an orthorhombic box with 100-Å cell edges for the structure factor calculation. Model Patterson vectors were selected according to length (between 24 and 4 Å) and according to peak height (3σ above the mean of the model Patterson map). The selected Patterson vectors were rotated using the Eulerian angles (θ_1, θ_2, θ_3) as defined in Rossmann and Blow (18). The product correlation with the Patterson map was computed by linear eight-point interpolation. The orientations of the search models were sampled by using the pseudo-orthogonal Eulerian angles (19): $\theta_+ = \theta_1 + \theta_3$; $\theta_- = \theta_1 - \theta_3$; and $\theta_2 = \theta_2$. The interval Δ for θ_2 was set to 2°. The interval for θ_+ is given by $\Delta/\cos(\theta_2/2)$, and the interval for θ_- is given by $\Delta/\sin(\theta_2/2)$. As the GDP[β,γ-CH_2]P-complex crystal symmetry is monoclinic $P2_1$, c-axis unique, the rotation search could be restricted to the asymmetric unit $\theta_+ = 0 - 720°$, $\theta_2 = 0 - 180°$, $\theta_- = 0 - 180°$ (20).

After the rotation function was calculated and a simple peak search was carried out, the 120 highest rotation function peaks were chosen. These are shown in Fig. 1*a*. The highest peak of the rotation function had a value 3.4 times the SD above the mean and 0.4 SD above the next highest peak. This orientation was consistently the highest peak for the data within the resolution ranges of 15–4 Å, 15–3.5 Å, and 15–3 Å. However, no other significant and consistent peaks could be located for the remaining three molecules despite variation of the parameters of the rotation function, such as resolution range and selection of Patterson vectors. The failure of the rotation search is not due to the choice of rotation function:

††The atomic coordinates for alpha carbons have been deposited in the Protein Data Bank, Chemistry Department, Brookhaven National Laboratory, Upton, NY 11973 (reference 4P21).

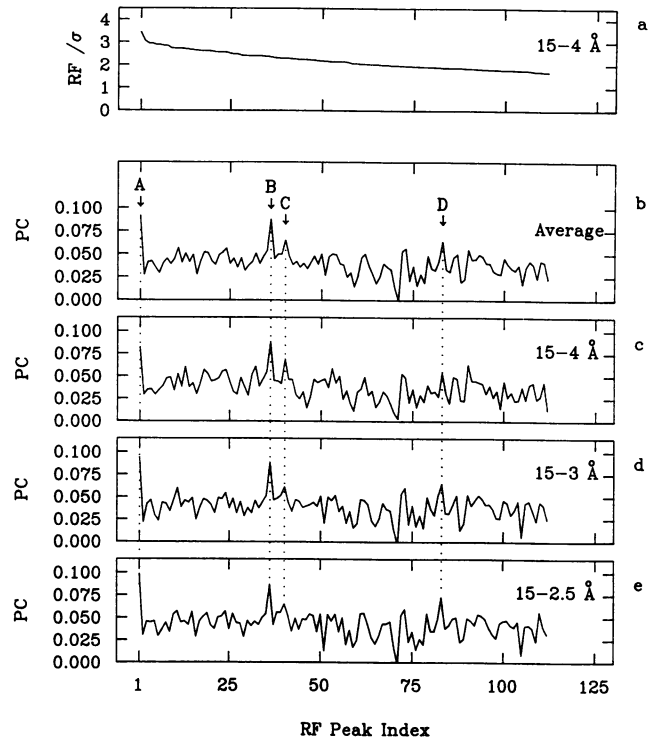

FIG. 1. By using the crystal structure of the GDP complex of normal human HRAS p21 catalytic domain minus GDP and residues 30–40 and 60–70 as probe, a rotation search was performed on diffraction data of the GDP[β,γ-CH_2]P complex of the protein. Values of the 120 highest peaks of the real-space rotation function (RF) are sorted by value (units of SDs above mean) (*a*). Rigid-body PC refinements were done for each orientation of the probe model corresponding to the 120 highest selected peaks of the rotation function. PC coefficients after the refinement are shown as 15- to 4-Å resolution (*c*), 15- to 3-Å resolution (*d*), and 15- to 2.5-Å resolution (*e*). (*b*) Average of *c*, *d*, and *e*.

equally inconclusive results were obtained using the rotation search program MERLOT (21).

Patterson Correlation (PC) Refinement of Rotation Function. To find the other orientations for the remaining three molecules in the asymmetric unit, another method, PC refinement of the orientation (16), was used. This refinement of the orientation (Ω) of the probe model is defined as minimization against a target function that consists of the following:

$$\varepsilon_{tot}(\Omega) = [1 - PC(\Omega)], \qquad [1]$$

where

$$PC(\Omega) = \frac{\langle|E_{obs}|^2|E_m(\Omega)|^2 - \langle|E_{obs}|^2\rangle\langle|E_m(\Omega)|^2\rangle\rangle}{\sqrt{(\langle|E_{obs}|^4 - \langle|E_{obs}|^2\rangle^2\rangle)(\langle|E_m(\Omega)|^4 - \langle|E_m(\Omega)|^2\rangle^2\rangle)}} \qquad [2]$$

The symbol $\langle\rangle$ denotes an averaging over the set of observed reflections expanded to the hemisphere of the reciprocal space corresponding to the triclinic space group P_1. E_{obs} and $E_m(\Omega)$ stand for, respectively, the normalized observed structure factors and the normalized structure factors calculated for the probe model oriented according to Ω and placed in a triclinic unit cell identical in geometry to that of the crystal.

The PC refinements consisted of 20 steps rigid-body conjugate gradient minimization (22) of ε_{tot} at 15- to 4-Å resolution (Fig. 1*c*), followed by 15 steps at 15- to 3-Å resolution (Fig. 1*d*), and, finally, 15 steps at 15- to 2.5-Å resolution (Fig. 1*e*) for each of the 120 selected peaks. The grid size for the fast Fourier transform evaluation of the structure factors was

FIG. 2. Tetramer formed by the GDP[β,γ-CH_2]P complex; thin lines represent the α carbon trace. The GDP[β,γ-CH_2]P ligand is shown as thick lines.

set to one-third of the high-resolution limit. Fig. 1*b* is the average of Fig. 1 *c*, *d*, and *e*.

Apart from peak number 1 (labeled A), a second strong peak emerged after PC refinement, which is labeled B. Peaks A and B are related by the noncrystallographic symmetry element $\psi = 66.5$, $\phi = -6.3$, $\kappa = 90.6$ (Table 1). Two additional peaks were located (labeled C and D), which were relatively consistent among resolution ranges. The four peaks are the largest peaks in the average plot (Fig. 1*b*). The correctness of peaks C and D is supported by the fact that they are approximately related to peaks A and B, respectively, by the element $\psi = 60.0$, $\phi = 0.0$, $\kappa = 180$ that was seen in the self-rotation function (Table 1). It should be noted that some peaks that were initially far away from the A, B, C, and D peaks converged to those peaks during the PC refinement. In particular cases, shifts of >50° in angular parameters were seen. These "redundant" peaks have been omitted on Fig. 1. These peaks can sometimes cause confusion in the interpretation of plots of the type of Fig. 1.

Translation Search. Translation searches were done by using the above-mentioned probe molecule oriented according to A, B, C, and D orientations (Table 1). The translation searches employed the standard linear correlation coefficient between the normalized observed structure factors and the normalized calculated structure factors (16, 23). The translation function TF(xyz, Ω) is defined as a function identical to PC(Ω), defined earlier except that $E_m(\Omega)$ is replaced by $E_{calc}(xyz, \Omega)$, where the latter denotes the normalized calculated structure factor for the probe and its symmetry mates, the center of gravity of which is located at position (x, y, z) and the orientation of the probe defined by Ω. The 15–4 Å resolution data were used, and the sampling interval was 1 Å in each dimension. The translation search was performed by first finding the location for the molecule A; then the positions of molecules B, C, and D were determined while keeping molecule A fixed. To check consistency, the procedure was repeated starting with molecule B fixed first and then placing A, C, and D and so forth. Significant and consistent positions emerged for all four molecular orientations (Table 2). The initial R factor of the combined four molecules was 40.7% at a resolution of 5–4 Å, which corresponded to a correlation coefficient of 0.48.

Structure Refinement. In addition to GDP, two additional parts were deliberately removed from the probe molecule during initial refinement: they were residues 30–40 and residues 60–70. The reason for deleting these residues was that the two regions were expected to be near the γ phosphate of the GDP[β,γ-CH_2]P, and we suspected that these regions may have conformations different from that of the probe molecule. Rigid-body refinements of the positions and orientations of the four molecules were accomplished by running 30 steps of conjugate gradient minimization at 5- to 4-Å resolution followed by 30 steps at 5- to 2.5-Å resolution. The R factor after rigid-body refinement was 37.8% at 5- to 4-Å resolution and 44.4% at 5- to 2.5-Å resolution. The four molecules form a tetramer that consists of two dimers (A, D and B, C) rotated by ≈90° (Fig. 2). The dimer symmetry axis is approximately the same for both molecules. This tetramer packing showed no close contacts among symmetry-related molecules and is very similar to that of four molecules related by the crystallographic symmetry found in the crystal structure of the intact human HRAS protein (unpublished result). However, two dimers are related to each other by ≈90° rotation, and the rotation axis is not quite parallel to the local 2-fold axis relating two dimers. This explains why no 4-fold noncrystallographic symmetry axis was found.

At this point [F(obs) − F(calc)] difference electron density maps were calculated. The maps clearly showed electron density corresponding to the four GDP[β,γ-CH_2]P molecules that were not present in the probe molecule and were not included in the calculation of structure factors. After fitting the GDP[β,γ-CH_2]P molecules to each of the four sites, one round of simulated annealing refinement (24) was carried out by using a slow cooling protocol (31). In this round of annealing tight noncrystallographic symmetry restraints (32) between the monomers were applied. The R factor dropped to 27% at 6- to 2.5-Å resolution with rms deviations of bond lengths and bond angles from ideality of 0.023 Å and 3.8°, respectively. The rms difference between the noncrystallographic symmetry-related monomers was 0.16 Å and 0.46 Å for the backbone and side-chain atoms, respectively. At this point [2F(obs) − F(calc)] electron density maps were calculated, and residues 30–40 and 60–70 were fitted into the maps; also, a magnesium ion was located in each of the four molecules. A subsequent round of simulated annealing refinement with noncrystallographic-symmetry restraints was carried out. Finally, the restraints were removed, and another cycle of simulated annealing refinement reduced the R factor to 19.5% for data with a resolution range of 5–2.5 Å and 20.4% for

Table 1. Orientation and symmetry relationship

	Before PC refinement			After PC refinement						
Molecule	θ_1	θ_2	θ_3	θ_1	θ_2	θ_3	Molecule pair	ψ*	ϕ*	κ*
A	105.2	102.0	53.7	104.9	102.2	55.4	A vs. B	66.5	−6.3	90.6
B	21.9	72.0	228.8	18.5	73.6	227.9	A vs. C	71.4	7.8	−91.6
C	199.5	110.0	72.5	201.1	112.6	77.3	A vs. D	63.9	1.6	179.3
D	284.2	80.0	256.2	286.0	80.6	252.2	B vs. C	62.2	3.8	179.2

*Spherical polar angles representing rotation required to rotate the first molecule onto the second molecule. The crystallographic symmetry operator ($-x$, $-y$, $z+1/2$) has been applied to molecules B and D.

Table 2. Translation searches

Molecule*	TF_{max}†	x‡	y‡	z‡	Peak height§		
					Correct	Error	S/N
A	0.14	−14.6	34.7	0.1	5.8	3.6	1.6
A+B	0.28	26.8	22.9	51.8	14.0	5.4	2.6
A+C	0.25	−18.3	43.8	25.6	12.3	4.6	2.7
A+D	0.23	32.0	11.7	75.1	10.9	4.9	2.2
B	0.15	26.7	22.7	51.8	6.8	3.4	2.0
B+A	0.29	−14.3	34.3	0.6	14.6	5.4	2.7
B+C	0.25	−18.5	44.0	26.3	11.0	4.1	2.6
B+D	0.24	32.1	11.7	76.0	11.7	4.7	2.4

*Molecule with which the translation search is done. When two molecules are specified, the first molecule is placed according to the translation search with that molecule alone and the search is done with the second molecule.
†Maximum correlation coefficient of the translation search. TF, translation function.
‡Position of molecule that yields maximum correlation coefficient in orthogonal Å coordinates.
§Peak heights are measured in σ units above mean. S/N, ratio of peak heights.

10–2.5 Å data at the present time. All computations were carried out with the program X-PLOR (25).

Description of Structure

The topological structure of the GDP[β,γ-CH_2]P complex is identical to that found for the GDP complex (10). The overall structure and many structural details are also the same as those of the GDP complex (8–10), except for two regions, residues 30–37 and 60–76. A stereoview of the backbone structure is shown in Fig. 3, where the two regions are indicated by the darker lines. The structural features of this complex are similar, except for residues 61–65, to those of another complex recently determined, a complex between p21 protein lacking the C-terminal 23 residues and another nonhydrolyzable GTP analog, GDP[β,γ-NH]P. The latter structure has been refined to an R factor of 22.9% at 2.6-Å resolution (11). The residues 61–65 are in weaker electron-density regions in both structures. Like the crystal structures of the GDP complex of the catalytic domain of human HRAS protein (8–10), the structure of the GDP[β,γ-CH_2]P complex consists of six β-strands forming a central sheet and five α-helices distributed on both sides of the β-sheet. There are 10 loops connecting the β-strands and α-helices.

FIG. 3. A stereoview of the α carbon positions of normal human HRAS p21 catalytic domain. Conformational differences between GDP and GDP[β,γ-CH_2]P complexes of the protein are primarily localized in two regions of the molecule; α carbon positions of these two regions are shown in thick lines. Numbers represent residues.

Common Features. Residues 14–17 tightly wrap around the β phosphate forming hydrogen bonds by using backbone NH groups exclusively (Figs. 3 and 5). The conformation of this region of the GDP complexes (26) is identical to that of the GDP[β,γ-CH_2]P complex. The most common oncogenic mutation site, residue 12, is located at the beginning of this loop. The environment of the magnesium ion is also shown in Fig. 5. It is coordinated by four oxygens, one each from the β phosphate, the γ phosphate, and the side chain of Thr-35 and

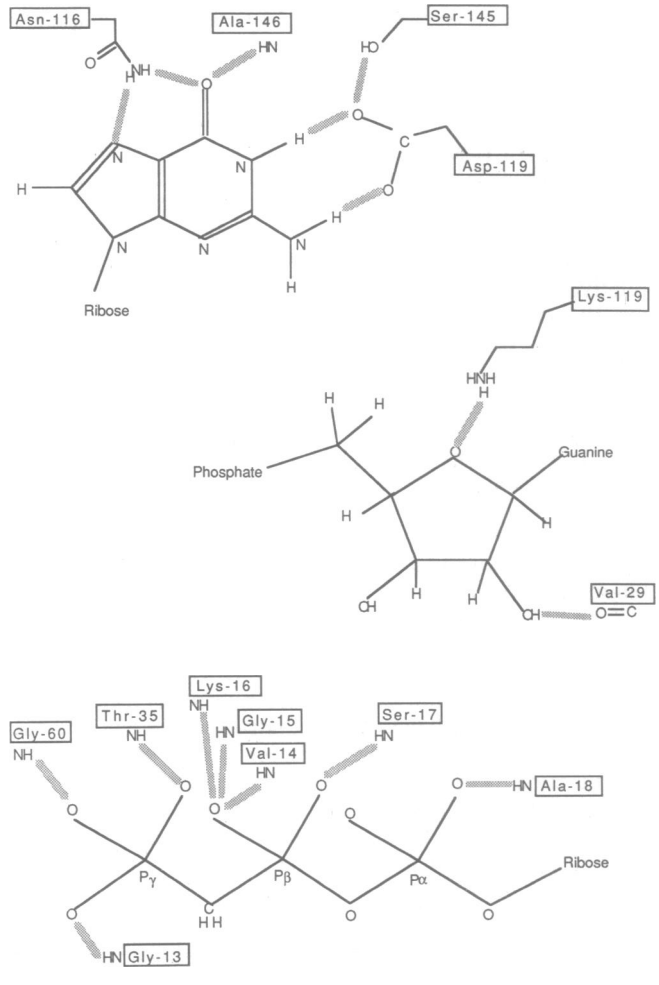

FIG. 4. Schematic of the hydrogen-bonding scheme of guanosine, ribose, and (β,γ-methylene)triphosphate found in the crystal structure GDP[β,γ-CH_2]P complex of normal human HRAS p21 catalytic domain. Interaction between protein and GDP portion of the nucleotide is conserved. Presumed hydrogen bonds at current resolution and refinement are indicated by wide shaded bands. Side chains that form hydrogen bonds to GDP[β,γ-CH_2]P are shown as attached to the respective amino acid by connected line segments. Backbone NH and CO groups that form hydrogen bonds are shown without connecting lines. The hydrogen bonding of Lys-119 to N3 of guanine and Gln-61 to γ-PO_4 is uncertain.

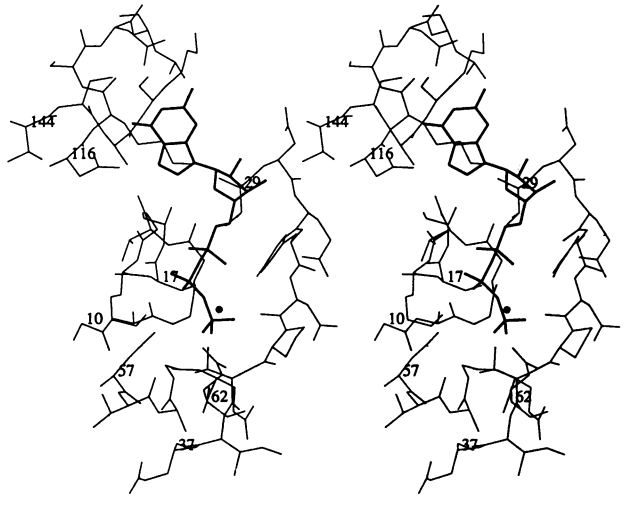

FIG. 5. Stereoview of the guanine nucleotide pocket at the current state of the refinement of the GDP[β,γ-CH_2]P complex of human normal HRAS p21 catalytic domain. GDP[β,γ-CH_2]P is shown by thick lines, and Mg^{2+} is shown as a small sphere.

Ser-17. The hydrogen-binding scheme of the guanine base and ribose is also shown in Fig. 4.

Thus all structural features involving the GDP portion of GDP[β,γ-CH_2]P in this complex are identical to those in GDP complexes and presumably conserved in all RAS protein structures so far determined. Most of these features are also found in the GDP[β,γ-NH]P complex (11).

Environment of the γ Phosphate. In analogy to the mechanism of GTP hydrolysis in EF-Tu (27), the γ phosphate of GTP in the complex with p21 protein is the most likely target of a nucleophilic attack by a water molecule (28). This suggests that the orientation of the γ phosphate is critical in the hydrolysis of GTP. Similar to GDP[β,γ-NH]P complex (11), our structure shows that the γ phosphate is held by four separate parts of the molecule (Figs. 4 and 5): The Mg^{2+} ion forms a coordination bond; the backbone NH group of residue 11 forms a hydrogen bond; the backbone NH group of residue 60 in loop 4 forms a hydrogen bond; and the backbone NH group of Thr-35 forms a hydrogen bond. Although further refinement of the structure may alter some of the bonding assignment, it is clear that many parts of the molecule participate in fixing the orientation of the γ phosphate.

Discussion

At the current resolution and refinement there appear to be two major consequences due to the presence of the γ phosphate as compared with the structures of GDP complexes (8–10, 26). (*i*) Extensive conformational changes occur in two regions of the molecule; residues 30–37 and residues 60–76 (Fig. 3). This correlates well with the observations that the mutations in the first region, the putative effector-binding site (29), alter the transforming properties of the proteins (1) and GAP binding (6, 7) and that mutations around residue 61 alter GAP binding strength (7). Furthermore, residue 61 (1) is also a common oncogenic mutation site. (*ii*) The locations of the β phosphate and magnesium ion appear to be slightly different when compared with those in the GDP complexes. This may be due to the fact that, in the GDP complexes, the magnesium ion is coordinated to the oxygen of β phosphate, whereas in the GDP[β,γ-CH_2]P complex it is coordinated to the oxygen atoms of both the β and γ phosphates in addition to that of Thr-35. Further refinement at higher resolution may resolve this issue.

The structural comparison also provides a preliminary structural basis for understanding biological and biochemical consequences of oncogenic mutations (1) at positions 12, 13, 61, 116, and 119 and of *in vitro* mutations of residues 30–40 and 59–62 and identifies regions of the molecular surface that are likely targets for interaction with membrane-bound components of *RAS*-mediated signal transduction (30). Although these structures suggest explanations for many biochemical and biological observations about RAS proteins, understanding the true mechanism of the biological functions of the proteins require structural studies of other complexes such as GTP analog complexes of oncogenic RAS proteins, GDP and GTP analog complexes of intact (full-length) RAS proteins and viral ras proteins, ternary complexes of GTP analogs, RAS protein, and GAP, as well as biochemical and biological studies of other interacting components of the signal-transduction pathway.

This work has been supported by grants from the National Institutes of Health (CA45593), the Department of Energy (DE-AC03-76SF000098), and by the Ministry of Health and Welfare for a Comprehensive 10-Year Strategy for Cancer Control, Japan, and gifts to the University of California from Merck, Burroughs Wellcome, and Hoffmann–La Roche.

1. Barbacid, M. (1987) *Annu. Rev. Biochem.* **56,** 779–828.
2. Kaziro, Y. (1978) *Biochim. Biophys. Acta* **505,** 95–127.
3. Gilman, A. G. (1987) *Annu. Rev. Biochem.* **56,** 615–649.
4. Stryer, L. & Bourne, H. R. (1986) *Annu. Rev. Cell Biol.* **2,** 391–419.
5. Trahey, M. & McCormick, F. (1987) *Science* **238,** 542–545.
6. Trahey, M., Wong, G., Halenbeck, R., Rubinfeld, B., Martin, G. A., Ladner, M., Long, C. M., Crosier, W. J., Watt, K., Koths, K. & McCormick, F. (1988) *Science* **242,** 1697–1700.
7. Vogel, U., Dixon, R. A. F., Schaber, M. D., Diehl, R. E., Marshall, M. S., Scolnick, E. M., Sigal, I. S. & Gibbs, J. B. (1988) *Nature (London)* **335,** 90–93.
8. deVos, A. M., Tong, L., Milburn, M. V., Matias, P. M., Jancarik, J., Noguchi, S., Nishimura, S., Miura, K., Ohtsuka, E. & Kim, S.-H. (1988) *Science* **239,** 888–893.
9. Tong, L., deVos, A. M., Milburn, M. V., Jancarik, J., Noguchi, S., Nishimura, S., Miura, K., Ohtsuka, E. & Kim, S.-H. (1989) *Nature (London)* **337,** 90–93.
10. Tong, L., Milburn, M. V., deVos, A. M. & Kim, S.-H. (1989) *Science* **245,** 244.
11. Pai, E. F., Kabsch, W., Krengel, U., Holmes, K. C., John, J. & Wittinghofer, A. (1989) *Nature (London)* **341,** 209–214.
12. Miura, K., Inoue, Y., Nakamori, H., Iwai, S., Ohtsuka, E., Ikehara, M., Noguchi, S. & Nishimura, S. (1986) *Jpn. J. Cancer Res. (GANN)* **77,** 45–51.
13. Rossmann, M. G. (1979) *J. Appl. Crystallogr.* **12,** 225–238.
14. Steigemann, W. (1982) PROTEIN, A Package of Crystallographic Programs for Analysis of Proteins (Max Plank Inst. for Biochemistry, Martinsried, F.R.G.).
15. Rossmann, M. G., ed. (1972) *Int. Sci. Rev. Ser.* **13.**
16. Brünger, A. T. (1990) *Acta Crystallogr. Sect. A* **46,** 46–57.
17. Huber, R. (February 1985) in *Molecular Replacement*, Proceedings of the Daresbury Study Weekend, ed. Machin, P. A. (Sci. Eng. Res. Council, Librarian, Daresbury Lab., Daresbury, U.K.), pp. 58–61.
18. Rossmann, M. G. & Blow, D. M. (1962) *Acta Crystallogr.* **15,** 24–31.
19. Lattman, E. E. (1985) *Methods Enzymol.* **115,** 55–77.
20. Rao, S. N., Jih, J.-H. & Hartsuck, J. A. (1980) *Acta Crystallogr. Sect. A* **36,** 878–884.
21. Fitzgerald, P. (1988) *J. Appl. Crystallogr.* **21,** 273–278.
22. Powell, M. J. D. (1977) *Math. Programming* **12,** 241–254.
23. Fujinaga, M. & Read, R. J. (1987) *J. Appl. Crystallogr.* **20,** 517–521.
24. Brünger, A. T., Karplus, M. & Petsko, G. A. (1989) *Acta Crystallogr. Sect. A* **45,** 60–61.
25. Brünger, A. T. (1988) *X-Plor Manual* (Yale Univ., New Haven, CT), Version 1.5.
26. Tong, L. (1989) Ph.D. Thesis (Univ. of California, Berkeley).
27. Webb, M. R., Reed, G. H., Cooper, B. F. & Rudolph, F. B. (1984) *J. Biol. Chem.* **259,** 3044–3046.
28. Feuerstein, J., Goody, R. S. & Webb, M. R. (1989) *J. Biol. Chem.* **264,** 6188–6190.
29. Sigal, I. S., Gibbs, J. B., D'Alanzo, J. S. & Scolnik, E. M. (1986) *Proc. Natl. Acad. Sci. USA* **83,** 4725–4729.
30. Milburn, M. V., Tong, L., DeVos, A. M., Brünger, A. T., Yamaizumi, Z., Nishimura, S. & Kim, S.-H. (1990) *Science* **247,** 939–945.
31. Brünger, A. T., Krukowski, A. & Erickson, J. W. (1990) *Acta Crystallogr. Sec. A* **46,** in press.
32. Weis, W. I., Brünger, A. T., Skehel, J. J. & Wiley, D. C. (1990) *J. Mol. Biol.* **212,** 737–761.